www.amlett.com, www.vbripress.com/aml, DOI: 10.5185/amlett.2014.amwc1011 Published online by the VBRI press in 2014

Crystallization and grain growth behavior of La_2O_3-doped yttria-stabilized zirconia

Bulent Aktas[1*], Suleyman Tekeli[2], Serdar Salman[3]

[1]*Department of Mechanical Engineering, Harran University, 63300, Sanliurfa, Turkey*
[2]*Metallurgical and Materials Engineering Department, Gazi University, Ankara, Turkey*
[3]*Faculty of Engineering and Architecture, Mehmet Akif Ersoy University, Burdur, Turkey*

[*]Corresponding author. Tel: (+90) 414 3183000; Fax: (+90) 414 3183476; E-mail: baktas@harran.edu.tr

Received:17 September, Revised: 01 December 2013 and Accepted: 13 December 2013

ABSTRACT

The effect of La_2O_3 addition on the microstructure and grain growth behavior of yttria-stabilized zirconia (8YSZ) was investigated. To this end, 8YSZ was doped with 1–15 wt% La_2O_3 by means of colloidal processing, and then sintered at 1550 °C for 1 h. XRD results identified a dissolution limit of 5 wt% La_2O_3 in 8YSZ, the insoluble La_2O_3 at higher concentrations reacting with ZrO_2 during sintering to form a secondary $La_2Zr_2O_7$ phase. Both undoped and La_2O_3-doped 8YSZ specimens were annealed at 1400, 1500, and 1600 °C for 10, 50, and 100 h to induce grain growth. Grain growth measurement results showed that an increase in annealing temperature and holding time caused to grain growth in all specimens. Excessive grain growth was observed in the case of the undoped, and 1-5 wt% La_2O_3-doped 8YSZ specimens; however, the grain growth in 10 and 15 wt% La_2O_3-doped 8YSZ was inhibited by the formation of a pyrochloric $La_2Zr_2O_7$ secondary phase around the grains and grain boundaries of 8YSZ. Grain growth exponent (n) and activation energy (Q) values for grain growth of undoped 8YSZ were obtained as 3, and 358 kJ/mol, respectively, while 15 wt% La_2O_3 containing specimens had a grain growth exponent of 3, and activation energy of 413 kJ/mol. These results indicate that grain growth rate can be controlled by the addition of 10 or 15 wt% La_2O_3.

Keywords: Yttria-stabilized zirconia (8YSZ); pyrochloric $La_2Zr_2O_7$; grain growth; solid oxide fuel cell (SOFC).

Bulent Aktas is assistant professor at the Department of Mechanical Engineering in the Harran University, Sanliurfa, Turkey. He has received his Ph.D. degree from Marmara University in 2008. His main research interest is synthesis, mechanical and electrical properties of zirconia ceramics for solid oxide fuel cells.

Suleyman Tekeli is a professor at the Metallurgical and Materials Engineering Department in the Gazi University, Ankara, Turkey. His research interests: Fuel cells, engineering ceramics, powder metallurgy, superplastic deformation, composite materials, excessive deformation methods. He has managed many research projects and published many research articles in international journals.

Serdar Salman is a professor at the Department of Mechanical Engineering in the Mehmet Akif Ersoy University, Burdur, Turkey and he is Dean of the Faculty of Engineering and Architecture. His research interests:Ceramic coatings, ceramics, biomaterials, destructive material testing methods, metallography, materials science. He published two books on materials science. He has published many research articles in international journals.

Introduction

Zirconia (ZrO_2)-based oxide ceramics are one of the best known and most widely used oxygen ion conductors employed in commercial fuel cells, oxygen sensors, and oxygen pumps **[1]**. Pure ZrO_2 is an insulating material that undergoes a number of phase transformations upon heating, it exists as monoclinic crystal from room temperature to 1170 °C, above which the monoclinic zirconia (m-ZrO_2) transforms into a tetragonal crystal structure; this transformation is accompanied by a volume reduction of 5%. At around 2370 °C, the tetragonal crystal structure transforms into cubic crystal structure. This cubic zirconia (8YSZ) is stable up to 2680 °C, which is the melting temperature of zirconia. The volume change caused during the phase transformations induces a large amount of stress, which tends to crack ZrO_2 upon cooling from high temperatures **[2]**. Consequently, ZrO_2 is typically blended with lower-valence oxides such as CaO **[3]**, Y_2O_3 **[4]**, Gd_2O_3 **[5]**, Sc_2O_3 **[6]** and La_2O_3 **[7]** to form a solid solution.

Pyrochlore $R_2Zr_2O_7$ (R = rare-earth-metal) compounds have been used as hosts for fluorescence centers and oxidation catalysts, and thus, a number of investigations have been conducted to evaluate the electrical, optical, and

catalytic properties of such materials **[8–10]**. Particular attention has been given to the pyrochlore $La_2Zr_2O_7$, which has been found to form at the cathode ($La_{1-x}Sr_xMnO_3$) / electrolyte (yttria-stabilized zirconia: YSZ) interfaces of solid oxide fuel cells (SOFCs) during high-temperature processing **[11, 12]**. This phenomenon has been investigated as a means of synthesizing $La_2Zr_2O_7$ by a number of different methods, including solid-state reaction **[13, 14]**, nitric acid dissolution, and the sol-gel technique **[13, 15, 16]**. However, the formation of pyrochlore $La_2Zr_2O_7$ has thus far only been achieved by the sol–gel process **[15]**. The ZrO_2–La_2O_3 system therefore not only provides stabilization of high-temperature structures, but also includes the pyrochloric-structured $La_2Zr_2O_7$ **[17, 18]**. This means it has potential for application as both a catalyst **[10]** and a thermal barrier **[19]**, and it can also be synthesized by either a solid-state reaction between oxides at 1500–1600 °C, or by the sol–gel process **[15]**.

In the case of solid-state reaction, grain growth occurs in ceramics during the sintering and high-temperature annealing processes. Since the mechanical properties of coarse-grained ceramics are lower than those of fine-grained ones **[20–23]**, a number of methods have been developed to prevent grain coarsening and to stabilize the microstructure. These prevent grain growth by making composite ceramics containing additives that facilitate sintering, in addition to using a cold and hot isostatic pressing processes **[24]**. It has been previously reported that the excessive grain growth in yttria-stabilized cubic zirconia (8YSZ) is associated with a low rate of Y_2O_3 precipitation at the grain boundaries. This in turn leads to a low cohesive strength between grain boundaries and a high grain boundary energy in the 8YSZ **[25]**. Consequently, in order to prevent grain growth, grain boundary mobility must be prevented and the grain boundary energy of the 8YSZ must be reduced. 8YSZ is well known for its high ionic conductivity and chemical stability across a range of different temperatures and oxygen partial pressures **[26]**; thus, it is widely used as an oxygen sensor **[27, 28]** and as a solid electrolyte in SOFCs **[29]**. In such applications, there is need not just for high conductivity, but also for greater mechanical, chemical, and electrical stability **[30]**. Due to the need for a high operating temperature (1000 °C) in SOFCs, the operating efficiency is greatly reduced **[31]**. Furthermore, the mechanical strength of 8YSZ is also reduced as a result of holding at high temperatures for long periods of time, which greatly restricts the use of the material as a solid electrolyte. These heat stresses, combined with the mechanical stresses caused by working and excessive grain growth, mean that 8YSZ used under such conditions tends to break quite easily **[32]**. Improving the mechanical properties of 8YSZ for use a solid electrolyte is therefore an important problem that still needs to be solved.

Consequently, the objective of this study is to prevent grain growth of 8YSZ through the addition of La_2O_3, thus improving its mechanical properties and suitability for use as a solid electrolyte. The choice of La_2O_3 as a dopant was based on the mismatch between the ionic radii of ZrO_2 and La_2O_3, and the fact that their valences are nearly equal. The effect of varying the amount of La_2O_3 addition on the phase equilibrium, microstructure, sintering, and grain growth of 8YSZ was subsequently investigated.

Experimental

Materials

For the matrix, 8 mol% of high-purity (>99.999%) 0.3 μm yttria-stabilized cubic zirconia (8YSZ) (Tosoh, Japan) powder was used, while up to 15 wt% of high-purity (>99.9%) 0.25 μm La_2O_3 (Mhc Industrial Co., China) powder was used as an additive. The chemical compositions of each powder are listed in **Table 1**.

Table 1. The chemical composition of the powders used in the experimental works.

	wt%								
Powders	ZrO_2	Y_2O_3	La_2O_3	TiO_2	FeO_2	Na_2O_3	CaO	Al_2O_3	SiO_2
8YSZ	85.9	13.6	-	0.1	0.003	0.01	0.02	0.25	0.1
La_2O_3	-	-	99.99	-	0.003	-	0.005	-	0.002

Colloidal processing and production of samples

The specimens for microstructural investigation were produced by means of colloidal processing. The doping process was carried out in a plastic container through the mechanical mixing of 8YSZ and up to 15 wt% La_2O_3 with zirconia balls and ethanol. The mechanical mixing was performed in a "speks" type mixer at 200 rpm for 12 h. The prepared slurries were left to dry for 24 h by simply leaving the mixer lid open. Once dry, the agglomerated powders with medium hardness were ball milled for 10 minutes to obtain a good dispersion and to break up the agglomerates. The resultant powders were passed through a 60 μm sieve and then pressed under 200 MPa of pressure in a single-axis die with a radius of 10 mm and a height of 4 mm. The inner surface of the steel die was cleaned after each dry-pressing process and stearic acid was applied to the side walls of the die as a release agent.

Sintering and density measurement of samples

Sintering was carried out in a box-type furnace under normal atmospheric conditions. The pressed pellets were first subjected to a pre-sintering process at 1000 °C, and then sintered at a temperature 1550 °C for 1 h with a heating and cooling rate of 5 °C /min. The density of the sintered specimens was calculated by assuming a perfect shape and using the rule of mixtures, while the ratio between weight and volume was determined by a geometrical method. The relative density was estimated on the assumption that the sintered body was of a cubic phase, and based on the theoretical densities of 5.68 and 6.51 g cm^{-3} for 8YSZ and La_2O_3, respectively.

XRD analysis and microstructural characterization

XRD (Shimadzu XRD 6000, CuK_α, λ = 1.5405 Å) was used to determine the probable changes in the crystal structure and lattice parameters of 8YSZ specimens up to 15 wt% La_2O_3. All samples were tested across a scan range of 0–70° at a scan speed of 0.03 °/s, and the resulting diffraction angles were measured. The grain growth of

specimens sintered at an optimum temperature was evaluated by annealing at 1400, 1500, and 1600 °C for 10, 50, and 100 h. The surfaces of the specimens were ground and polished using normal metallographic methods after sintering, and were then thermally etched by holding in a furnace at 50 °C below the sintering temperature for 1 h. The microstructural investigation of the sintered specimens was performed using a scanning electron microscope (SEM, Jeol Lv 6060). The grain sizes of the specimens were measured by the mean linear intercept method and the average for each specimen was determined using the following equation:

$$D = \frac{L_i}{N_i . M} \quad (1)$$

where L_i is the length of the line, N_i is the number of grain-boundary intercepts, and M is the magnification in the photomicrograph of the material.

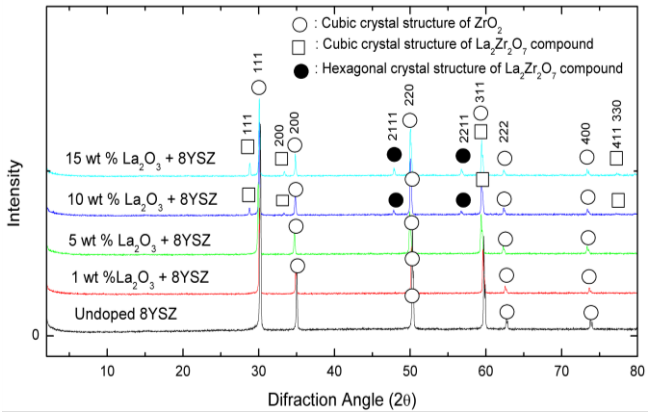

Fig. 1. XRD patterns of undoped and La_2O_3-doped 8YSZ specimens.

Results and discussion

Fig. 1 shows the XRD patterns obtained from 8YSZ specimens doped with various amounts of La_2O_3. From this, it can be seen that those specimens containing 1 and 5 wt% La_2O_3 are composed of only a single cubic-structured crystal phase. Furthermore, no La_2O_3 peaks were observed in these specimens, indicating that La_2O_3 was completely dissolved in the 8YSZ matrix and did not remain as a secondary phase around the grains or grain boundaries of 8YSZ. However, when more than 5 wt% La_2O_3 is added, peaks emerge corresponding to pyrochloric $La_2Zr_2O_7$ that indicate the overdoped La_2O_3 is not solubilized in the 8YSZ matrix, but rather forms a secondary $La_2Zr_2O_7$ phase at high temperatures.

SEM and EDS analyses revealed that this new phase is preferentially precipitated around the grains and grain boundaries of 8YSZ. Moreover, the XRD results show that the $La_2Zr_2O_7$ is composed of hexagonal and cubic crystal structures. Some of the peaks of the 8YSZ specimens doped with 10 and 15 wt% La_2O_3 can be indexed to a cubic-pyrochlore-structured $La_2Zr_2O_7$ and a hexagonal-crystal-structured $La_2Zr_2O_7$, which is in agreement with JCPDS 30-1468 and JCPDS 17-0450 (International Center for Diffraction Data Files). The formation of pyrochloric $La_2Zr_2O_7$ is likely due to the difference in the ionic radii and crystal structures of La^{3+} and Zr^{4+} ions; it is well-known that the ionic radius of La^{3+} with a hexagonal structure is 1.016 Å, while that of Zr^{4+} with a cubic crystal structure is 0.84 Å. The pyrochloric structure is therefore defined as two distinct and intertwined structures that are distinguished as a cation-centered octahedral ZrO_6 and an anion-centered tetrahedral La_4O. The $La_2Zr_2O_7$ is formed by the unification of one tetrahedral and two octahedral structures, with La^{3+} cations situated in a hexagonal window of the octahedral lattice **[32, 33]**.

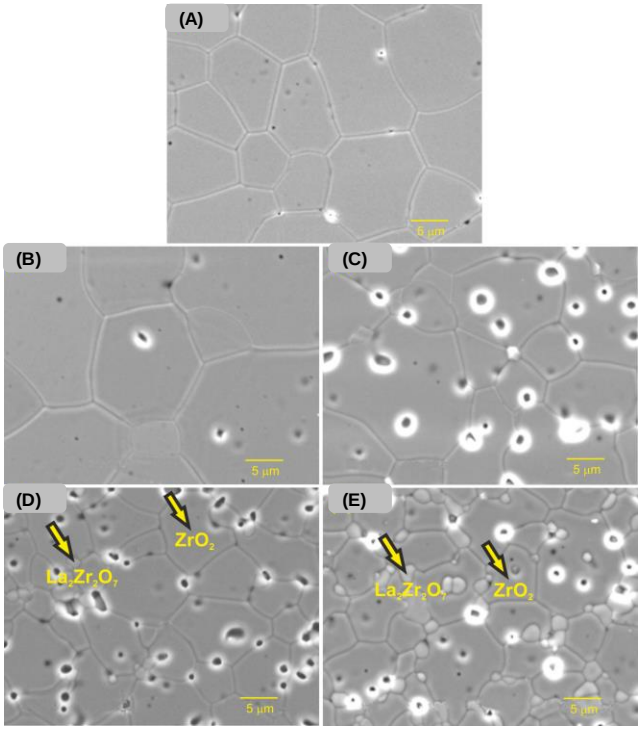

Fig. 2. The microstructures of the undoped and the different amounts of La_2O_3-doped 8YSZ specimens annealed at 1500 °C for 100 h. (A) Undoped, (B) 1, (C) 5, (D) 10 and (E) 15 wt% La_2O_3-doped 8YSZ.

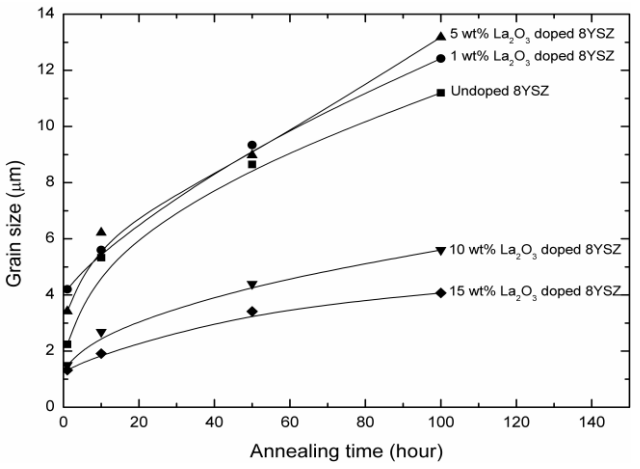

Fig. 3. The grain sizes of the undoped and with various amounts of La_2O_3-doped 8YSZ specimens after annealing at 1500 °C for 10, 50 and 100 h.

The microstructures of the undoped La_2O_3-doped 8YSZ specimens annealed at 1500 °C for 100 h are presented in **Fig. 2.** This shows that grain growth did occur in the undoped and La_2O_3-doped 8YSZ specimens, with the rate

of growth increasing annealing temperature and holding time. The undoped 8YSZ specimen and those doped with 1 and 5 wt% La_2O_3 exhibit an equiaxed, faceted, uniform, and coarse-grained structure (**Fig. 2A-C**), whereas those samples with 10 and 15 wt% La_2O_3 have faceted 8YSZ grains, together with smaller spherical grains of $La_2Zr_2O_4$ (**Fig. 2D-E**). Furthermore, it can be observed in **Fig. 2** that the porosity level increases with increasing La_2O_3 content.

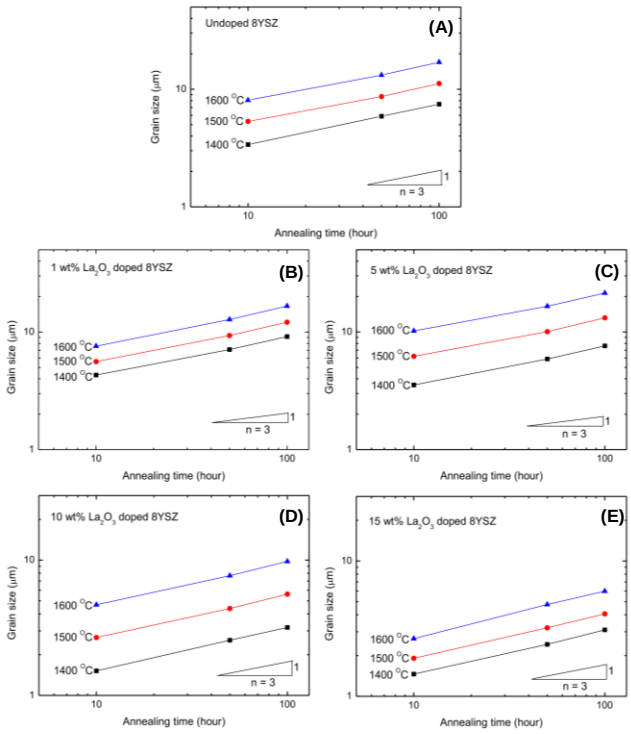

Fig. 4. The grain growth exponent values for the undoped and La_2O_3-doped 8YSZ at different temperatures and holding times.

The grain sizes of the specimens doped with various amounts of La_2O_3 after annealing at 1500 °C for 10, 50, and 100 h are presented in **Fig. 3.** This reveals that there was grain coarsening in the undoped 8YSZ and in 1 and 5 wt% La_2O_3-doped 8YSZ after annealing; the grain growth in the 1 and 5 wt% La_2O_3-doped 8YSZ was greater than that in undoped 8YSZ, because of the high diffusion coefficient and dissolution of La_2O_3 in the 8YSZ matrix. Grain growth in the 10 and 15 wt% La_2O_3-doped specimens was notably reduced by the presence of the secondary $La_2Zr_2O_7$ phase around the grains and grain boundaries, resulting in a much finer-grained structure.

Grain growth kinetics was determined using the following equations:

$$D^n - D_0^n = K(t - t_0) \quad (2)$$

$$K = K_0 \exp\left(-\frac{Q}{RT}\right) \quad (3)$$

where D is the grain size after a period of time t, D_0 is the initial grain size, n is the grain growth exponent, K is a kinetic constant dependent on grain boundary and temperature, K_0 is a constant not dependent on temperature and Q, R and T are activation energy, gas constant and the absolute temperature, respectively. The grain growth exponent (n) is calculated from the slope of the line obtained from a plot of log (D)-log(t), as shown in **Fig. 4**.

The grain growth exponent (n) values of undoped and La_2O_3-doped 8YSZ specimens are given in **Fig. 4**, and these vary depending on the specimen microstructure **[34]**. The value of n is generally between 2 and 4, and when equal to 2, it exhibits a parabolic relationship in single-phase systems at high temperature. Grain growth is controlled by solid solution drag when the value of n is 3, the necessary conditions for which are that one of the components of solid solution should precipitate at the grain boundaries. When the value of n is 4, it indicates that the grain growth rate is controlled by pore drag; however, considered highly unlikely to be the case in this instance given the narrow grain size distribution and small porosity fraction (2–4 %) **[35]**. The values of n for the undoped and La_2O_3-doped 8YSZ specimens were subsequently calculated as 3 (**Figure 4A-E**), indicating an impurity drag controlled growth mechanism.

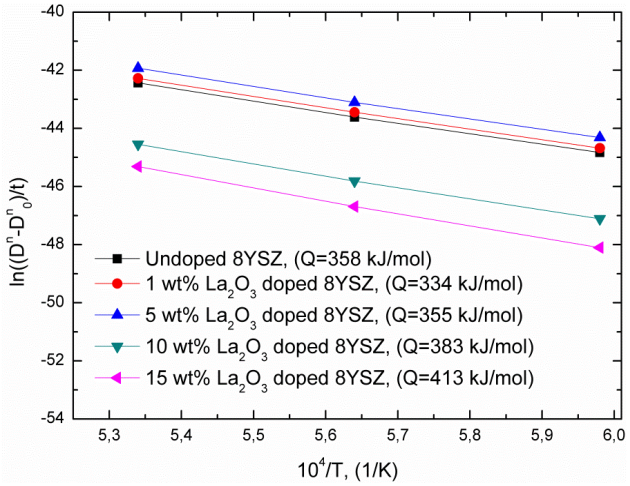

Fig. 5. The grain growth activation energies of undoped and La_2O_3-doped 8YSZ specimens.

The activation energy, Q, for the grain growth was calculated from the slope of the line obtained from a plot of $\ln((D^n - D^n_0)/t)$ vs $1/T$, as shown in **Fig. 5**. These results reveal that the activation energies of 10 and 15 wt% La_2O_3-doped 8YSZ specimens are substantially higher than those of undoped 8YSZ, which is believed to be due to $La_2Zr_2O_7$ secondary phase. A higher activation energy means a lower rate of grain growth. The activation energy for undoped 8YSZ was calculated as 358 kJ/mol, whereas the activation energies for 1, 5, 10, and 15 wt% La_2O_3-doped 8YSZ specimens were calculated as approximately 334, 355, 383, and 413 kJ/mol, respectively. It can therefore be seen that the activation energies of the 1 and 5 wt% La_2O_3-doped 8YSZ specimens are in fact lower than that of undoped 8YSZ, which means that grain growth should be faster in 1 and 5 wt% La_2O_3-doped 8YSZ specimens. This reduced activation energy in the 1 and 5 wt% La_2O_3-doped 8YSZ specimens is likely to be attributable to the high diffusion coefficient and rate of dissolution of La_2O_3 in the 8YSZ matrix.

Conclusion

XRD analysis showed that the 8YSZ specimens doped with 1 and 5 wt% La_2O_3 have a cubic crystal structure, and that this structure did not change with the addition of La_2O_3. Furthermore, these specimens did not exhibit La_2O_3 peaks, indicating that the La_2O_3 was completely dissolved in the 8YSZ matrix. However, with an increase in doping to more than 5 wt%, peaks corresponding to pyrochloric $La_2Zr_2O_7$ emerged that indicate the excess La2O3 forms a secondary phase of $La_2Zr_2O_7$ at high temperatures.

Increasing the annealing temperature and holding time caused increased grain growth in both undoped and La_2O_3-doped 8YSZ specimens. Excessive grain coarsening was observed in the undoped, 1 and 5 wt% La_2O_3-doped 8YSZ specimens; however, grain growth in the 10 and 15 wt% La_2O_3-doped 8YSZ specimens was inhibited by the presence of the $La_2Zr_2O_7$ secondary phase around the grains and grain boundaries of 8YSZ. The grain growth exponent values (n) of the undoped and La_2O_3-doped 8YSZ specimens obtained were found to be equal to three, indicating that grain growth was controlled by impurity drag. The activation energies for the 1, 5, 10, and 15 wt% La_2O_3-doped 8YSZ specimens were determined to be 334, 355, 383, and 413 kJ/mol, respectively. The activation energy was particularly increased in the 10 and 15 wt% La_2O_3-doped 8YSZ, confirming a reduction in grain growth when compared to undoped 8YSZ.

Acknowledgements

Authors thank Gazi University and Marmara University, TURKEY, for the provision of laboratory facilities.

Reference

1. Zhang, T.; Zeng, Z.; Huang, H.; Hing, P.; Kilner, J., *Mater. Lett.*, **2002**, 57, 124. **DOI:** 10.1016/S0167-577X(02)00717-6
2. Badwal, S.P.S.; *Solid State Ionics*, **1992**, 52, 23. **DOI:** 10.1016/0167-2738(92)90088-7
3. Ho, S.M.; *Mater. Sci. Eng.*, **1982**, 54, 23.
4. Ramsmoorthy, R.; Ramasamy, S.; Sundararaman, D., *J. Mater. Res.*, **1999**, 14, 90. **DOI:** 10.1557/JMR.1999.0015
5. Muccillo, E.N.S.; Rocha, R.A.; Muccillo, R., *Mater. Lett.*, **2002**, 53, 353. **DOI:** 10.1016/S0167-577X(01)00506-7
6. Badwal, S.P.S.; Drennan, J., *Solid State Ionics*, **1992**, 53–56, 769. **DOI:** 10.1016/0167-2738(92)90253-L
7. Arachi, Y.; Sakai, H.; Yamamoto, O.; Takeda, Y.; Imanishai, N., *Solid State Ionics*, **1999**, 121, 133. **DOI:** 10.1016/S0167-2738(98)00540-2
8. Otaki, H.; Kido, H.; Hoshikawa, T.; Shimada, M.; Koizumi, M., *Nippon Seram. Kyo. Gak.*, **1988**, 96, 124. **DOI:** 10.2109/jcersj.96.124
9. McCauley, R.A.; *J. Opt. Soc. Am.*, **1973**, 63, 721. **DOI:** 10.1364/JOSA.63.000721
10. Korf, S.J.; Koopmans, H.J.A.; Lippens, B.C.; Burggraaf, A.J.; Gellings, P.J., *J. Chem. Soc. Faraday Trans. I*, **1987**, 83, 1485. **DOI:** 10.1039/f19878301485
11. Echigova, J.; Ohfuji, T.; Suto, H., *J. Mater. Sci. Lett.*, **1994**, 13, 1098. **DOI:** 10.1007/BF00633525
12. Setoguchi, T.; Inoue, T.; Takebe, H.; Eguchi, K.; Morinaga, K.; Arai, H., *Solid State Ionics*, **1990**, 37, 217. **DOI:** 10.1016/0167-2738(90)90247-O
13. Poulsen, F.W.; Puil, N., *Solid State Ionics*, **1992**, 53/56, 777. **DOI:** 10.1016/0167-2738(92)90254-M
14. Labrincha, J.A.; Marques, F.M.B.; Frade, J.R., *J. Mater. Sci.*, **1993**, 28, 3809. **DOI:** 10.1007/BF00353183
15. Kido, H.; Komarneni, S.; Roy, R., *J. Am. Ceram. Soc.*, **1991**, 74, 422. **DOI:** 10.1111/j.1151-2916.1991.tb06899.x
16. Matsumura, Y.; Yoshinaka, M.; Hirota, K.; Yamaguchi, O., *Solid State Commun.*, **1997**, 104, 341. **DOI:** 10.1016/S0038-1098(97)00332-3
17. Schneider, S.J.; Roth, R.S.; Waring, J.L., *J. Res. Natl. Bur. Stand. Sect. A*, **1961**, 65A, 345. **DOI:** 10.6028/jres.065A.037
18. Rouanet, A.; *Rev. Int. Hautes Temp. Refract.*, **1971**, 8, 161.
19. Cao, X.Q.; Vassen, R.; Jungen, W.; Schwartz, S.; Tietz, F.; Stover, D., *J. Am. Ceram. Soc.*, **2001**, 84, 2086. **DOI:** 10.1111/j.1151-2916.2001.tb00962.x
20. Wang, J.; Rainforth, M.; Stevens, R., *Br. Ceram. Trans.*, **1989**, 88, 1.
21. Eichler J.; Rodel, J.; Eisele, U.; Hoffman, M., *J. Am. Ceram. Soc.*, **2007**, 90, 2830. **DOI:** 10.1111/j.1551-2916.2007.01643.x
22. Casellas, D.; Alcala, J.; Llanes, L.; Anglada, M., *J. Mater. Sci.*, **2001**, 36, 3011. **DOI:** 10.1023/A:1017923008382
23. Trunec, M.; *Ceram. Silik.*, **2008**, 52, 165.
24. Tekeli, S.; Boyacioglu, T.; Gural, A., *Ceram. Int.*, **2008**, 34, 1959. **DOI:** 10.1016/j.ceramint.2007.07.003
25. Tekeli, S.; *J. Alloys Compd.*, **2005**, 391, 217. **DOI:** 10.1016/j.jallcom.2004.08.084
26. Bamba, N.; Choa, Y.H.; Sekino, T.; Niihara, K., *J. Eur. Ceram. Soc.*, **1998**, 18, 693. **DOI:** 10.1016/S0955-2219(97)00192-1
27. Maskell, W.C.; *Solid State Ionics*, **2000**, 134, 43. **DOI:** 10.1016/S0167-2738(00)00712-8
28. Riegel, J.; Neumann, H.; Wiedenmann, H.M., *Solid State Ionics*, **2002**, 152–153, 783. **DOI:** 10.1016/S0167-2738(02)00329-6
29. Minh, N.Q.; *J. Am. Ceram. Soc.*, **1993**, 76, 563. **DOI:** 10.1111/j.1151-2916.1993.tb03645.x
30. Zhang, T.; Zeng, Z.; Huang, H.; Hing, P.; Kilner, J., *Mater. Lett.*, **2002**, 57, 124. **DOI:** 10.1016/S0167-577X(02)00717-6
31. Tekeli, S.; Demir, U., *Ceram. Int.*, **2005**, 31, 973. **DOI:** 10.1016/j.ceramint.2004.10.011
32. Hyde, B.G.; Thompson, J.G.; Withers, R.L., *Mater. Sci. and Tech. A*, **1994**, 11, 35.
33. Fuertes, M.C.; Porto Lopez, J.M., *Ceram. Int.*, **2004**, 30, 2137. **DOI:** 10.1016/j.ceramint.2003.11.020
34. Lin, Y.J.; Angelini, P.; Mecartney, M.L., *J. Am. Ceram. Soc.*, **1990**, 73, 2728. **DOI:** 10.1111/j.1151-2916.1990.tb06753.x
35. Sagel-Ransijn, C.D.; Winnubst, A.J.A.; Burggraaf, A.J.; Verweij, H., *J. Eur. Ceram. Soc.*, **1997**, 17, 1133. **DOI:** 10.1016/S0955-2219(96)00217-8